ELSEVIER

Contents lists available at ScienceDirect

Journal of Hydrology

journal homepage: www.elsevier.com/locate/jhydrol

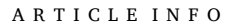


Research papers

Water-table response to extreme precipitation events

Claudia R. Corona a,*, Shemin Ge a, Suzanne P. Anderson a,b

- ^a University of Colorado, Boulder, Department of Geological Sciences, Boulder, CO, USA
- b Institute of Arctic and Alpine Research, Boulder, CO, USA



Keywords:
Extreme precipitation events
Water-table response
HYDRUS-1D
Inverse modeling
Hydraulic diffusivity

ABSTRACT

Extreme precipitation events (EPEs) will play a significant role in influencing soil—water and groundwater storage worldwide. We examined water-table depth (WTD) response to EPEs for 17 cases representative of soils and climate settings across the United States. Precipitation data from NOAA's Precipitation Frequency Data Server were used for each case to characterize 1-day extreme precipitation events (EPEs) with annual exceedance probabilities of 0.1 % over an average baseline date range of 1981–2011. The inverse solution in the HYDRUS-1D modeling software was used to obtain the soil—water retention curve for each case. Non-EPE and EPE scenarios were modeled and compared to examine water-table displacement (Δ_{WTD}) and recession time (t_{rec}). The Δ_{WTD} ranged from 0.6 to 2.4 m across cases and were not directly controlled by EPE amount; instead, Δ_{WTD} was inversely related to available porosity. Soils with low available porosity experienced large Δ_{WTD} compared to soils with higher available porosity. In cases with larger diffusivity values, the modeled water table receded faster than in cases with smaller diffusivity values. This was because water-table recession times, t_{rec} , were inversely related to hydraulic diffusivity. For all cases, recession back to pre-EPE levels ranged from months to years suggesting an increased role by the unsaturated zone in buffering EPEs that should be considered in future EPE-groundwater modeling studies.

1. Introduction

Communities worldwide depend on groundwater for water needs in urban, rural, industrial and agricultural settings (Alley, 2002; Wu et al., 2002; Miguez-Macho et al., 2007). In the United States alone, groundwater use increased by 8 % while surface-water use decreased by 14 % from 2010 to 2015 (Dieter et al., 2018; Maupin, 2018). In an average precipitation year, groundwater use is offset by the replenishment of groundwater stores due to infiltration from precipitation (Freeze, 1969; Vereecken et al., 2015). The rate of infiltration is controlled by the subsurface soil (rock) physical properties, such as the medium's water content, soil porosity, and soil hydraulic conductivity, all of which influence the timing and distribution of infiltration through the unsaturated zone and to the water table (Freeze and Cherry, 1979).

Traditional theory suggests that low-intensity precipitation events over long periods can lead to a constant rate of infiltration through the subsurface that is ideal for replenishment of groundwater stores (Freeze and Cherry, 1979). However, it remains unclear how the subsurface will

respond to climate change, which is expected to cause a decline in low-intensity precipitation events (Lehmann et al., 2015; Li et al., 2019; Myhre et al., 2019) and cause an increase in shorter, more extreme (higher-intensity) precipitation events (Westra et al., 2013; Prein et al., 2017; Pendergrass and Knutti, 2018; Sun et al., 2021). A climatic change towards shorter, more extreme precipitation events (EPEs) is likely to affect subsurface response, which, combined with increased economic reliance on groundwater, may exacerbate the strain on groundwater resources (Wilkinson and Cooper, 1993; Green et al., 2011; Dieter et al., 2018).

The potential influence of an EPE on subsurface response can be illustrated by comparing water-table response to two rainfall scenarios, differing only by the addition of an EPE (Fig. 1). Recall that water table fluctuates over time, generally rising towards the surface with large infiltration events, then decreasing once precipitation stops (Freeze and Cherry, 1979). In the non-EPE scenario (Fig. 1b), the water table fluctuates in response to average precipitation. Addition of an EPE (Fig. 1c) may result in a large influx of infiltrating water and rapid water-table

Abbreviations: EPE, extreme precipitation event; UNSODA, Unsaturated Soil hydraulic Database; BcCZO, Boulder Creek Critical Zone Observatory; NOAA, National Oceanographic Atmospheric Administration; AEP, annual exceedance probability; WTD, water table depth.

E-mail address: claudia.corona@colorado.edu (C.R. Corona).

https://doi.org/10.1016/j.jhydrol.2023.129140

^{*} Corresponding author.

displacement towards shallower depths, before receding over time to non-EPE water table levels. Water-table displacement and recession time (Fig. 1c) after an EPE can provide insightful understanding of subsurface response to EPEs.

Only recently have the effects of EPEs on groundwater recharge been the subject of field and modeling campaigns (Wang et al., 2015; Thomas et al., 2016; Wittenberg et al., 2019; Golian et al., 2021). For example, rapid transmission of infiltrating water from EPEs to the water table has been detected through stable isotopic composition of precipitation and groundwater in the tropics (Jasechko and Taylor, 2015) and the North China Plain (Zheng et al., 2019). Many studies have focused on determining links between precipitation patterns and recharge during EPEs (Tashie et al., 2016; Golian et al., 2021; Boas and Mallants, 2022). In contrast, fewer studies have considered subsurface conditions, which include soil properties, and their effect on EPE-induced recharge (Crosbie, 2003).

Studies that have addressed subsurface response to EPEs have generated somewhat conflicting results. Examining subsurface response to EPEs in differing semi-arid basin sites, Crosbie (2003) identified a positive correlation between water table depth and recharge, where recharge increased with depth to the water table. They found that recharge amount generally increased with precipitation amount (Crosbie, 2003). For example, at one field site, they found that 200 mm of monthly rainfall resulted in monthly recharge of 100 mm, while 450 mm of monthly rainfall resulted in monthly recharge of 250 mm (Crosbie, 2003). Tashie et al. (2016) identified a positive correlation between recharge and precipitation event duration across a sub-tropical region, and an inverse correlation between recharge and the average rate of precipitation during the event. Where Crosbie (2003) found that recharge increased with depth to the water table, Tashie et al. (2016) found no relation between recharge and depth to water table in the subtropical study area. Golian et al. (2021) considered recharge timing and precipitation amount using the groundwater balance equation and water-table fluctuation method (Healy and Cook, 2002), finding that water-table response to EPEs across the semi-arid and arid field sites was delayed by 6-months. This is in contrast to the faster, days-long response identified in other semi-arid and arid climates (Crosbie, 2003), humid continental climates (Joachim et al., 2011) and sub-tropical climates (Tashie et al., 2016). The differing results of EPE impacts on water tables across varying soils and climate conditions warrants further study. Mathematical models that use existing soil data to examine physical responses to EPEs could help clarify many of these divergent findings (Vereecken et al., 2015).

Mathematical models have been used along with local climate data to explore the effects of EPEs on groundwater recharge. Using the Soil Water Balance (SWB1) model (Westenbroek et al., 2010), Zhang et al. (2016) found that EPEs accounted for a greater fraction of recharge in the Northern High Plains Aquifer ($\sim\!60$ %) compared to average precipitation events, despite comprising <40 % of the total precipitation from 1950 to 2010. While the study did not simulate unsaturated flow, the results showed that more of the infiltration from the EPE became potential recharge compared to average precipitation events, highlighting the importance of EPEs (Zhang et al., 2016). Scanlon et al. (2018) compared regional-scale groundwater level changes between land surface models and remote sensing products, finding that the models underestimated large decadal water storage trends, both increasing and decreasing, relative to the remote sensing product. It was suggested that the discrepancies between the model results and satellite data was due to a lack of representing unsaturated zone processes and soil properties in the land surface models (Scanlon et al., 2018).

To consider the climactic influence on subsurface response, studies have used HYDRUS-1D (Simunek et al., 2005), a one-dimensional unsaturated-saturated flow model capable of modeling vadose zone processes (Leterme et al., 2012; Boas and Mallants, 2022; Corona and Ge, 2022). Leterme et al. (2012) used HYDRUS-1D to examine the effects of climate change on groundwater recharge near a disposal facility for radioactive waste, and found that recharge would decrease in some areas near the disposal site but increase slightly at another nearby site over the next 10,000 years of climatic change. Focusing on an arid basin in central Australia, Boas and Mallants (2022) used HYDRUS-1D to estimate groundwater recharge from EPEs at a bare soil and vegetated site with statistically generated sets of hydraulic properties, finding that

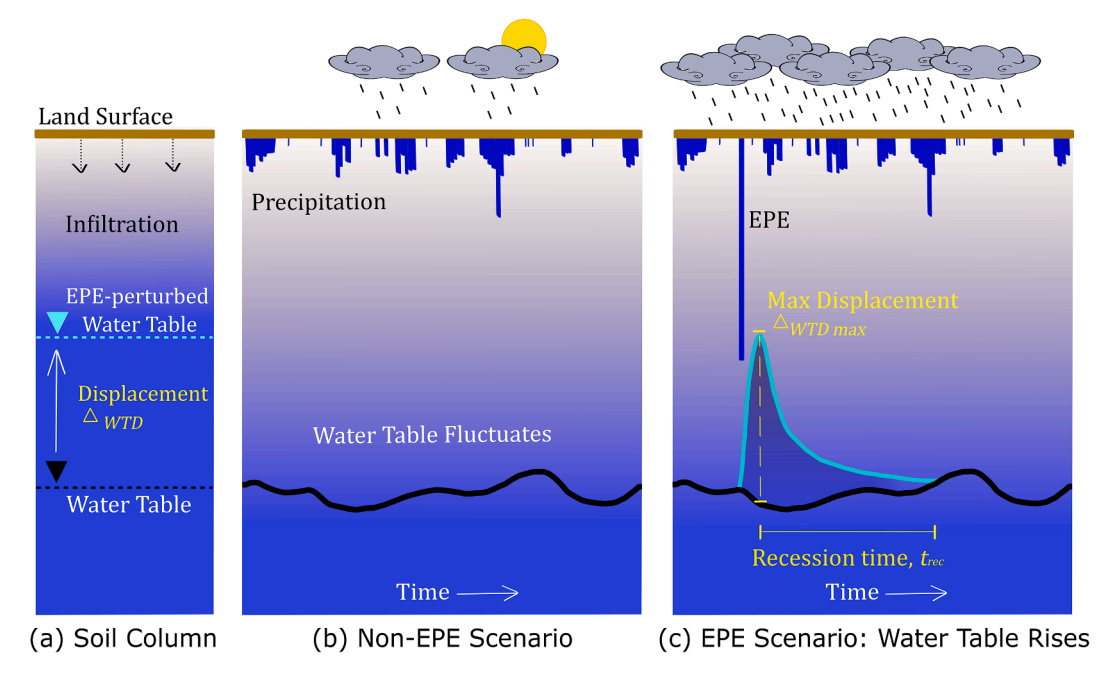


Fig. 1. Conceptual model showing: (a) model soil column, (b) Non-EPE scenario portraying the typical water-table fluctuations (black line) expected with normal precipitation patterns over time. (c) EPE scenario, contrasting the water-table response to an EPE (light blue line) with the non-EPE scenario (black line). Following the EPE, the water table was displaced upward, reaching a maximum ($\Delta_{WTD~max}$) relative to the non-EPE scenario. The recession time (t_{rec}) was defined as the time needed for water-table displacement to recede to within 5% of $\Delta_{WTD~max}$. (For interpretation of the references to colour in this figure legend, the reader is referred to the web version of this article.)

more recharge occurred at the bare soil site compared to the vegetated site after every EPE. Corona and Ge (2022) created a HYDRUS-1D model of the subsurface in a semi-arid region to examine water-table response to an EPE, finding that the water table remained elevated for at least 18 months after the event. To our knowledge, no study has yet to consider subsurface response to EPEs across various climates and soils.

As precipitation patterns shift to more extreme events (both droughts and EPEs alike), a knowledge gap remains regarding how unsaturated zone hydrological properties influence water-table response to EPEs. To address this knowledge gap, time series data about EPEs are needed, as well as soil hydrological properties. These data, coupled with a subsurface flow model which considers the physics of the unsaturated zone and water table dynamics provide a mechanism to investigate the subsurface response to EPEs. This study explored water-table response to EPEs in diverse settings, based on water-table response for 17 cases across the United States. First, we used water content as a function of pressure head data from the Unsaturated Soil hydraulic Database (UNSODA) with HYDRUS-1D inverse modeling to obtain the soil-water retention curves for the 17 cases. Second, we created two models for each case: a "non-EPE" scenario and an "EPE" scenario, which are used to explore the differences in water-table response. We address the following questions: (1) How does EPE amount impact water-table response? (2) How do properties of the unsaturated zone influence water-table response to EPEs? (3) How do properties of the saturated zone influence post-EPE water-table recession time?

2. Methods

2.1. Data collection

2.1.1. Soil hydraulic properties

Study cases are shown on a map of the principal aquifers of the United States (Fig. 2a) for reference (U.S. Geological Survey, 2003). We used soil hydraulic data from UNSODA, a database with field and lab measurements of soil properties, such as water content as a function of pressure head, hydraulic conductivity as a function of pressure head, soil bulk density, among other measurements, for sites in the United States (Nemes et al., 2001). Measurements from each UNSODA soil were used to construct case-specific soil characteristic curves (water content as a function of pressure head), and obtain the vertical saturated hydraulic

conductivity (K_s) for 14 of the 17 cases (Nemes et al., 2001). U.S. Geological Survey (USGS) data were used for the Mukilteo, WA case (Smith et al., 2017) and the Atlantic Highlands, NJ case (Fiore et al., 2021). Boulder Creek Critical Zone Observatory (BcCZO) data were used for the Betasso site (Anderson and Ragar, 2022).

We also plot the respective soil types onto a modified version of the U.S. Department of Agriculture's (U.S. Department of Agriculture, 1987) soil textural triangle classification system (Fig. 2b). Soil texture class was reported for each study case, but not detailed textural data. The symbols on the soil texture triangle (Fig. 2) therefore are only correct to the texture class level. The soil descriptions in the UNSODA database and the USGS reports suggest that twelve of the soils plotted are predominantly of a sandy texture, three soils are predominantly silty, and one soil is predominantly clay (Fig. 9). The AZ and CO cases are not plotted because the USDA textural triangle does not apply to rock materials (Garcia-Gaines and Frankenstein, 2015).

2.1.2. Daily precipitation

Daily precipitation data were sourced from the nearest precipitation station to each case location as described in Table 1. Precipitation stations are managed by the National Oceanographic and Atmospheric Administration (NOAA, 12 stations), the USGS (3 stations), the Colorado State University (1 station), and the BcCZO (1 station). The precipitation datasets used were 95 % complete or better for a continuous five-year period between 2000 and 2021.

2.1.3. Extreme precipitation events

The precipitation amount that constitutes an EPE can vary with climate (Perica et al., 2013). To maintain a uniform EPE definition across the diverse climates from which cases were derived, we define EPEs using precipitation-depth-frequency curves from the NOAA National Weather Service, Hydrometeorological Design Studies Center's Precipitation Frequency Data Server (NOAA, 2017). NOAA used a regional frequency analysis approach to calculate the annual percent chance of occurrence of precipitation amounts at a station (Perica et al., 2013). Only precipitation stations with a minimum of 30 data years were considered for calculations of annual exceedance probability (Perica et al., 2013). For the calculations of annual exceedance probability, the most recent precipitation date range considered by NOAA was 1981–2011. To conduct the analysis, first, the maximum precipitation

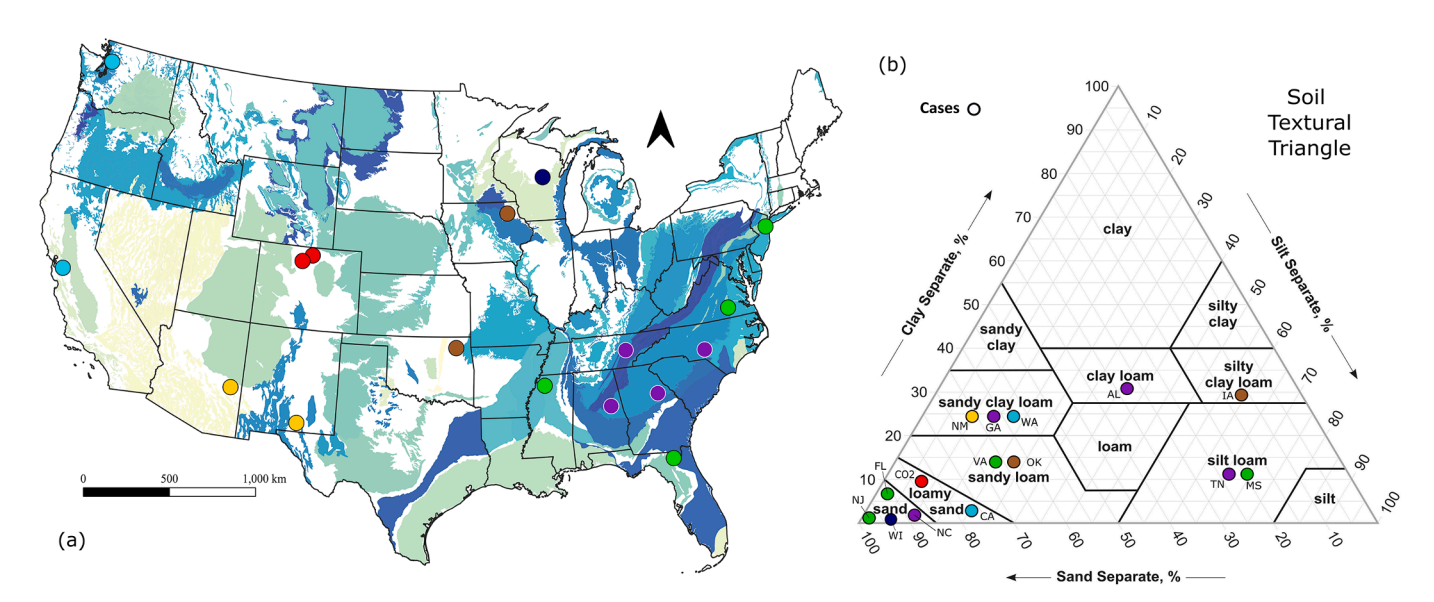


Fig. 2. (a) Approximate case locations (colored dots) across the United States. Principal aquifer systems are colored on the map for reference (USGS, 2003). (b) Black triangle delineates the 12 soil textural classes. Dots show soil texture class for soils used in this study, but do not specific clay-silt-sand percentages, which were not reported in site data. Not shown: AZ (tuffaceous rock) and CO (unweathered bedrock). Soil and climatic data cases are listed in Table 1. (For interpretation of the references to colour in this figure legend, the reader is referred to the web version of this article.)

Table 1

Case locations and precipitation stations organized longitudinally from west to east. The precipitation collection agency, station name, ID, and coordinates are provided.

Case Location	Case ID	Soil Data Source	Precipitation Station Name	Precipitation Station ID, Agency	Latitude (°)	Longitude (°)
Mukilteo, Washington	WA	USGS	Mukilteo Lighthouse Park	USGS	47.90	-122.33
Antioch, California	CA	UNSODA	Antioch Pump Plant #3	USC00040232, NOAA	37.99	-121.75
Superior, Arizona	AZ	UNSODA	Queen Valley 0.2 E	US1AZPN0077, NOAA	33.30	-111.29
Las Cruces, New Mexico	NM	UNSODA	Mesilla 2.3 E	US1NMQA0116, NOAA	32.27	-106.77
Betasso, Boulder County, Colorado	CO	BCCZO	Betasso	Boulder Creek CZO (BcCZO)	40.01	-105.33
Fort Collins, Colorado	CO2	UNSODA	Fort Collins	53005, CO State University	40.58	-105.09
Perkins, Oklahoma	OK	UNSODA	Perkins	USC00347003, NOAA	35.97	-97.03
Iowa State University, Iowa	IA	UNSODA	Turkey River, Spillville	431226091570101, USGS	43.21	-91.95
Hancock, Wisconsin	WI	UNSODA	Hancock Experimental Farm	USC00473405, NOAA	44.12	-89.54
Auburn, Alabama	AL	UNSODA	Auburn #2	USC00010425, NOAA	32.60	-85.47
Oak Ridge, Tennessee	TN	UNSODA	Oak Ridge ATDD	USW00003841, NOAA	36.00	-84.24
Watkinsville, Georgia	GA	UNSODA	Athens Ben Epps Airport	USW00013873, NOAA	33.95	-83.33
Laurinburg, North Carolina	NC	UNSODA	Laurinburg	USC00314860, NOAA	34.75	-79.47
Live Oak, Florida	FL	UNSODA	Live Oak 0.4 NE	US1FLSW0001, NOAA	30.30	-82.98
Panola County, Mississippi	MS	UNSODA	Batesville 2.2 SSE	US1MSPN0001, NOAA	34.29	-89.93
Blackstone, Virginia	VA	UNSODA	Fort Pickett	USC00441322, NOAA	37.04	-77.95
Atlantic Highlands, New Jersey	NJ	USGS	Mt. Mitchill Scenic Overlook (MMSO)	MMSO, USGS	40.41	-74.01

series per year (of a given duration, i.e., 24-hours) from a station was collected and merged with maximum precipitation series data (same duration) from 8 to 16 nearby stations. The collected data (for the station and its surroundings) was then used to calculate a regional average of maximum precipitation measured for the given duration (Perica et al., 2013). This regional average was weighted by the length of the available data record to create a set of data points that represented increasing precipitation amount for various exceedance probabilities. A cumulative distribution function, the Generalized Extreme Value distribution, was then fitted to the data (Perica et al., 2013). The Generalized Extreme Value distribution employs the maximum-likelihood approach for large samples to calculate the probability of exceedingly rare or extreme events (Hosking et al., 1985; Perica et al., 2013).

The National Weather Service, a subset of NOAA, conducted the procedure for each precipitation duration (i.e. 1-hour, 3-days, etc.) for all stations (Perica et al., 2013). The end product was a smooth curve relating precipitation depth (m) to annual exceedance probabilities (AEP). The AEP is the probability of a precipitation event exceeding a certain depth once or more in any given year (Hosking and Wallis, 1997; Perica et al., 2013). Fig. 3 shows AEPs ranging from 1/2 (50 % chance of

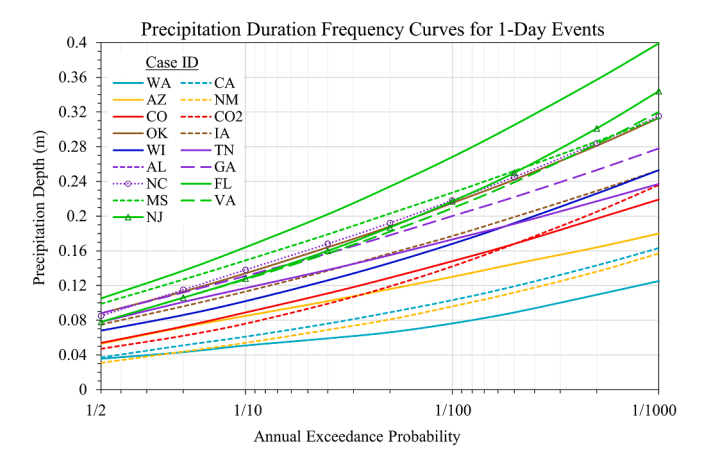


Fig. 3. Precipitation depth frequency curves for 1-day durations. On the x-axis, the Annual Exceedance Probabilities (AEPs) range from 1/2 (50% chance of occurrence in a year) to 1/1000 (0.1% chance of occurrence in a year) for the 17 cases. We use the 1-day precipitation depth frequency curve at the AEP of 1/1000 to define a case EPE. (For interpretation of the references to colour in this figure legend, the reader is referred to the web version of this article.)

occurrence) to 1/1000 (0.1 % chance of occurrence). To account for the spatial variability of precipitation from case to case, the EPE was defined as a 1-day (or 24-hour) precipitation event with a 0.1 % (1-in-1000 year) chance of occurrence (Fig. 3).

2.2. Subsurface flow modeling

2.2.1. Governing equation

The nonlinear nature of flow in the subsurface was considered by Richards (1931), who hypothesized that the pressure head (ψ) and unsaturated hydraulic conductivity (K) were both functions of the water content (θ) (Richards, 1931; Youngs, 1988). Ignoring thermal effects and air-phase flow, the one-dimensional Richards equation based on water balance takes the form:

$$\frac{\partial \theta}{\partial t} = \frac{\partial}{\partial z} \left[K \left(\frac{\partial \psi}{\partial z} + 1 \right) \right] \tag{1}$$

where θ is the water content, t is time (T), ψ is the pressure head (L), K is the unsaturated hydraulic conductivity (L/T), and z is the vertical coordinate representing depth below the surface (L). Numerical models such as HYDRUS-1D (Šimůnek et al., 2005) solve the Richards equation for pressure head distribution in an unsaturated–saturated porous medium. HYDRUS-1D employs the van Genuchten (1980) equations for soil hydraulic properties. Using a pore-size distribution model described by Mualem (1976), the van Genuchten-Mualem equations provide continuous functional relations for soil water retention, and the unsaturated hydraulic conductivity, of a soil (Mualem, 1976; van Genuchten, 1980). The water content and pressure head curve θ (ψ), is called the soil–water retention curve (SWRC):

$$\theta (\psi) = \begin{cases} \theta_r + \frac{\theta_s - \theta_r}{\left[1 + |\alpha \psi|^{nn}\right]^m} & \psi < 0 \\ \theta_s & \psi \ge 0 \end{cases}$$
 (2)

where θ_r and θ_s denote the residual and saturated water content, respectively, α is a parameter inversely related to the air-entry pressure, nn is a pore-size distribution index, and m is a parameter used to relate nn to K (Mualem, 1976; van Genuchten, 1980). The pore-size distribution index, nn, is the relative abundance of each pore size in a representative volume of soil (Nimmo, 2013). The nn typically ranges from 1 to 10: smaller nn (\sim 1.01) represents smaller pores and less variation in pore sizes, while larger nn (\sim 10) is descriptive of larger pores and greater variation in pore size (Cary and Hayden, 1973; van Genuchten, 1980; Šimůnek et al., 2005). Van Genuchten (1980) showed nn to be

smaller for clay soil and larger for sandier soils. The hydraulic conductivity-pressure head, $K(\psi)$ relation of a soil is given by:

$$K = K(\psi) = K_s S_e^l \left[1 - \left(1 - S_e^{\frac{1}{m}} \right)^m \right]^2$$
 (3)

$$m = 1 - \frac{1}{nn}, \ nn > 1 \tag{4}$$

where K_s is the saturated hydraulic conductivity (L/T), l is a poreconnectivity parameter (dimensionless) and S_e is the effective saturation, also dimensionless (Mualem, 1976; van Genuchten, 1980). The effective saturation (dimensionless), S_e , is calculated as:

$$S_e = \frac{\theta - \theta_r}{\theta_r - \theta_r} \tag{5}$$

For this study, the K_s for each case was obtained from the UNSODA catalog (Nemes et al., 2001). If UNSODA did not specify K_s for a case, the soil series from the UNSODA database was used in a query in USDA's National Resource Conservation Service online browser (NRCS, 2022a) to identify the possible K_s values. This was done for the IA (NRCS, 2022b), NM (NRCS, 2022c), OK (NRCS, 2022d), TN (NRCS, 2022e), and WI (NRCS, 2022f) cases. Based on the information provided in the soil series report, an average K_s value was assigned to the soil.

2.2.2. Model setup and assumptions

The model domain was set up as a 1D vertical column extending from the land surface to a depth of z = 50 m. A sensitivity study (not shown) of the effects of soil column length >40 m (i.e., 50 m, 60 m, 75 m, and 100 m) found no significant differences in model results. Thus, 50 m was chosen for the model domain. The model domain consisted of twolayers, with the top layer extending from z=0 to z=10 m, and the bottom layer extending from z = 10 m to z = 50 m. The soil column was discretized into 1000 elements of 0.05 m each. Soil hydrologic properties for each case were determined using the inverse estimation in HYDRUS-1D, which minimizes the summation of the squared differences between the observed water content values and the simulated water content values (Simunek et al., 2005). The best-fitting soil hydraulic parameters (θ_r , θ_s , α , and nn) were applied uniformly across both layers of the model domain for each case. The K_s value assigned to the bottom layer was smaller than the value assigned to the top layer, however, in order to represent the typical decrease in K_s with depth below the surface.

This 1D approach ignored lateral flow, topographic influence, and multi-layered heterogeneity, factors which influence long-term watertable fluctuations. For this study, 1D infiltration and diffusion were likely dominant processes. The 1D approach used here focused on the magnitude of the response to EPEs and time of recession with different hydraulic parameters during short-time periods. In contrast to the complications and added assumptions of 3D models, simple 1D models of systems can show generic responses to EPEs and other climate phenomena, allowing for attention to be focused on possible controlling factors that may otherwise be masked (Wilkinson and Cooper, 1993; Corona et al., 2018).

The top boundary condition at the land surface was set as an atmospheric boundary condition (i.e., precipitation over time, units: L/T) with surface runoff possible but without surface ponding. The bottom boundary condition was defined as a deep drainage flux. The downward drainage flux out of the column is generally at a distance away from the water table, where $q(\psi)$ was approximated by (Hopmans and Stricker, 1989):

$$q(\psi) = -Ae^{(B \mid \psi_{bottom} - GWL \mid)}$$
(6)

The $q(\psi)$ (L/T) was a flux crossing the bottom boundary. The A and B were adjustable empirical parameters, where A represents a rate (L/T) and B represents an inverse length (1/L) (Hopmans and Stricker, 1989;

Neto et al., 2016). The ψ_{bottom} (L) was the pressure head at the bottom boundary. *GWL* (L) was a reference pressure head at some distance away (Hopmans and Stricker, 1989); as a first-order approximation, we assumed that *GWL* = 50 m. The *A* parameter was related to the saturated hydraulic conductivity, K_s . The *B* parameter was calibrated iteratively to allow the water table to initialize at the desired water table depth (i.e., 5 m or 27 m) following the methodology of Neto et al. (2016) and Corona and Ge (2022).

We determined the model's initial conditions as follows. First, we assigned an initial pressure head distribution that linearly increased from $\psi = -5$ m at the surface (z = 0 m) to $\psi = 45$ m at the bottom of column (z = 50 m) for 16 of the 17 cases. Of the UNSODA soils, only the AL, WI, and GA cases had water table depth data, which was a limiting factor (Nemes et al., 2001). To compensate, the modeled water table was initialized at a 5 m depth for the 11 of 14 cases that did not have water table depth data. The steady-state water table for each case varied between 3 m and 9 m depth depending on case-specific soil properties and precipitation input. In the model, the unsaturated zone extended from the ground surface to a depth of \sim 5-9 m, where the water table was located. The saturated zone extended from the water table to the bottom of the soil column (z = 50 m). The top layer included unsaturated/ saturated conditions, while the bottom layer was fully saturated. To account for the deeper water table at Betasso, the model was initialized with a prescribed ψ distribution that increased linearly from $\psi = -27$ m at the surface (z = 0 m) to $\psi = 23$ m at the bottom (z = 50 m). The water table depth at the Betasso site was initialized at a depth of 27 m to reflect field measurements at the monitoring well (Anderson and Ragar, 2022).

For model spin-up, daily average precipitation minus evapotranspiration was used as the atmospheric boundary condition at the model top. We used existing regional estimates of evapotranspiration to determine a case-specific average (Sanford and Selnick, 2013; Reitz et al., 2017). The model spin-up served two purposes: 1) to allow the model to equilibrate to a steady state from which transient runs were executed, and 2) to iteratively calibrate the *B* parameter.

The resulting steady-state model was the starting condition from which transient conditions commence (i.e. variable precipitation is applied). The transient model used case-specific daily precipitation minus case-specific evapotranspiration. For cases with UNSODA and BcCZO soil data, the transient models employed a 5-year precipitation dataset. For cases with USGS soil data, the available precipitation dataset record (~2–5 years) was used. The transient model had two scenarios: a "non-EPE" scenario where only the non-EPE precipitation record was applied (Fig. 1b) and an "EPE" scenario that included a 1-day EPE near the beginning of the precipitation record (Fig. 1c). The results from the two scenarios were compared for each case to examine the differences in water-table response.

2.3. Water-table response: displacement and recession

Two aspects of water-table response were considered: water-table displacement, Δ_{WTD} , and the recession time, t_{rec} . Once the non-EPE scenarios and EPE scenarios were run, the respective water table depths from the model output were calculated. The water-table displacement, Δ_{WTD} , was calculated as the difference between the EPE and non-EPE modeled water table levels (m) computed at each time step. The maximum difference in water-table response between the EPE and non-EPE scenario was designated the Δ_{WTD} max. After max displacement, the water table remained elevated above non-EPE levels for varying amounts of time (months to years), eventually receding to non-EPE scenario simulation levels. The water-table recession time, t_{rec} , was defined as the time needed for water table-displacement, Δ_{WTD} to recede to within the 5 % of $\Delta_{WTD~max}$ (Fig. 1c). From a temporal perspective, this approach only focused on the period of response to EPEs and the subsequent recovery, which occurred within a few years and is not representative of long-term water-table fluctuations.

3. Results and discussion

To show an example of how the water table may respond to an EPE, we introduce data from the Betasso site in the Front Range of Colorado, part of the Boulder Creek Critical Zone Observatory (BcCZO). In 2013, a monitoring well at Betasso captured groundwater response to an EPE (Anderson et al., 2013; Langston et al., 2015), which we modeled using a 1D approach. Following the case study, subsequent sections discuss water-table displacement, Δ_{WTD} , and water-table recession time, t_{rec} , as a function of soil properties for all 17 cases. We note that while the soil types and EPE amounts presented were related to soil measurements and precipitation station data from various sites, these cases may apply to other sites provided similar conditions, such as: water table depths, EPE amounts, and geological materials.

3.1. Case study: Betasso, Boulder Creek Critical Zone Observatory

The Colorado Front Range experienced a catastrophic precipitation event that lasted a week in September 2013. The heaviest rain fell over a \sim 24-hour period several days into the storm, with local sustained rainfall rates of 25–50 mm/hour and 24-hour rainfall annual exceedance probabilities <1/1000 years (Gochis et al., 2015). The presence of colocated precipitation gages and monitoring wells for months before the storm afforded a rare opportunity to examine an extreme event in detail. Corona and Ge (2022) had previously modeled the Δ_{WTD} in response to this EPE at Gordon Gulch, a site \sim 10 km to the west of Betasso. At Gordon Gulch, the EPE resulted in water-table displacement of 1.50 m and recession time of \sim 18 months in a well with a water table at \sim 9 m depth (Corona and Ge, 2022). At the Betasso site, more rain was received during the 2013 EPE than the Gordon Gulch site. The groundwater level at Betasso rose \sim 2.4 m as the water table rose from \sim 27.5 m to 25.1 m (depth below land surface) over a period of about

fourteen days. We acknowledge that this was a rare case where the 1-Day EPE was preceded by two days of precipitation and followed by three more days of precipitation (Anderson et al., 2022). The purpose of this case study was to show how numerical models can adequately simulate field measurements that captured the water-table response to an EPE.

Fig. 4 compares water table depths modeled for an EPE and a non-EPE scenario with the measured water table depths at Betasso. The

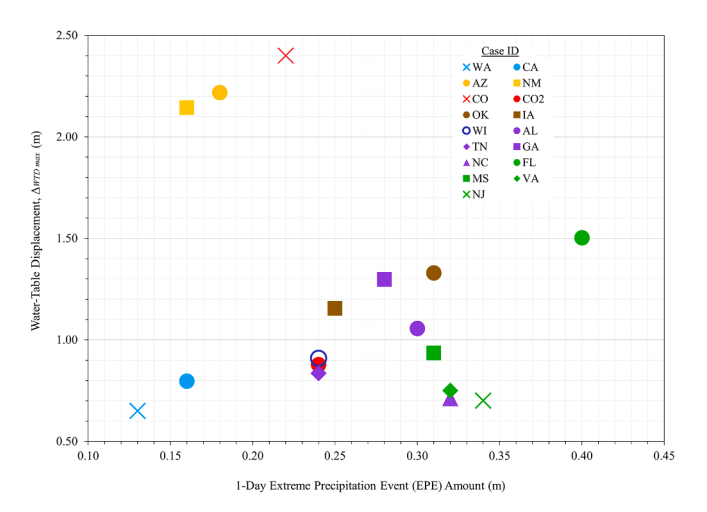


Fig. 5. Scatter plot showing modeled water-table displacement, $\Delta_{WTD~max}$ at 17 cases in response to 1-day EPE amounts. (For interpretation of the references to colour in this figure legend, the reader is referred to the web version of this article.)

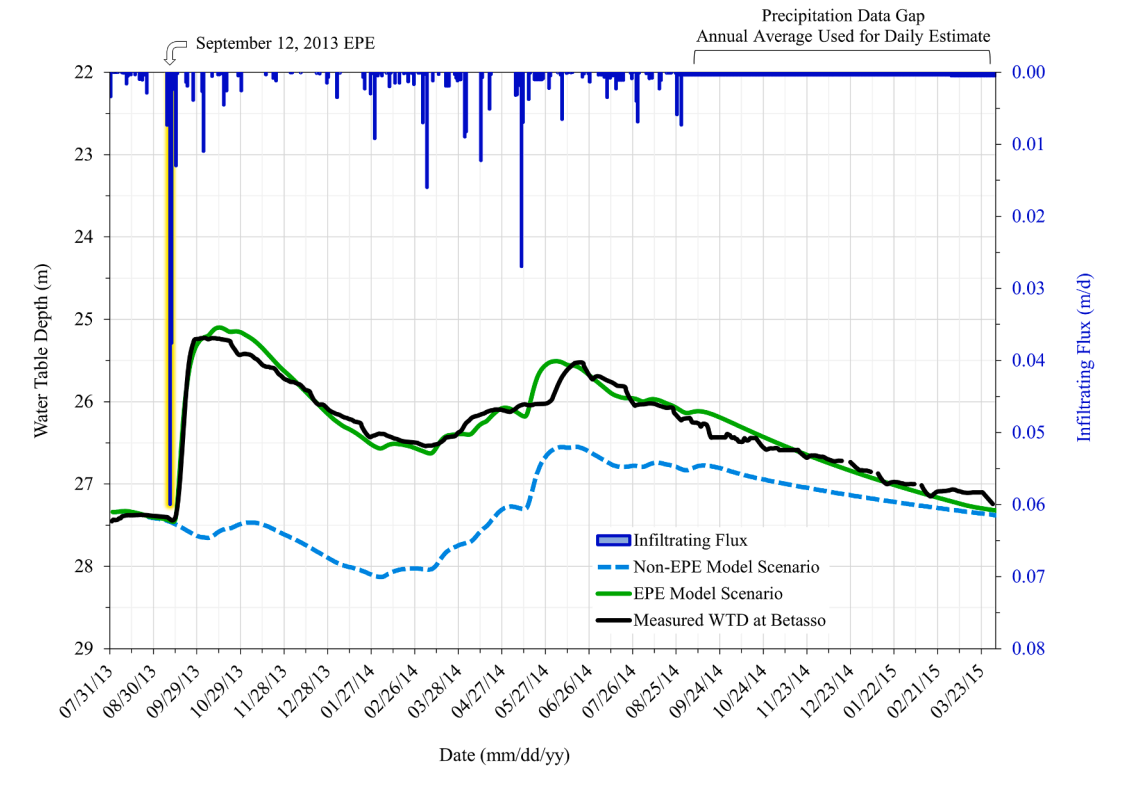


Fig. 4. Measured water-table depths at Betasso (black line) from August 2013 to April 2015, showing response to the September 2013 EPE. Modeled water table with EPE (green line) and the non-EPE (dashed blue line) scenarios shown. The infiltration flux (m/d) (dark blue line) was derived from a meteorological station at Betasso. The one-day September 12, 2013 EPE is highlighted in yellow. From September 2014 through early 2015, the Betasso meteorological station went offline for repairs. To compensate, the annual average precipitation amount was used to estimate daily precipitation minus evapotranspiration (0.00045 m/d) for the data gap. (For interpretation of the references to colour in this figure legend, the reader is referred to the web version of this article.)

Table 2 Precipitation station date range, EPE input amount, steady-state water table depth (m), modeled water table depth range (m), and $\Delta_{WTD \text{ max}}$ (m) for each model case.

Case ID	Precipitation Data, Date Range	EPE Amount (m)	Steady state Water Table Depth (m)	Modeled Range of Water Table Depth (m)	$\Delta_{WTD~{ m max}}$ (m)
WA	06/21/2015 - 07/05/2017	0.13	5.0	4.0 – 5.5	0.65
CA	10/01/2002 - 06/30/2021	0.16	5.9	4.8 – 6.5	0.80
AZ	05/01/2017 - 05/01/2022	0.18	7.0	4.5 - 8.0	2.22
NM	03/01/2010 - 03/01/2022	0.16	7.0	4.5 – 7.5	2.14
CO	06/01/2013 - 06/01/2019	0.22	27.4	25.0 – 28.0	2.40
CO2	09/01/2008 - 09/01/2021	0.24	5.0	4.0 – 5.3	0.88
OK	01/01/2013 - 07/31/2021	0.31	6.7	5.5 – 7.1	1.33
IA	12/01/2011 - 12/20/2020	0.25	5.2	4.2 - 5.6	1.16
WI	01/01/2010 - 02/04/2022	0.24	4.1	3.2 - 4.5	0.91
AL	01/01/2010 - 02/28/2022	0.30	4.9	3.5 - 5.2	1.06
TN	01/01/2000 - 08/31/2021	0.24	5.1	4.4 – 5.6	0.84
GA	05/01/2008 - 11/21/2021	0.28	8.8	8.0 - 9.4	1.21
NC	01/01/2000 - 10/30/2021	0.28	5.0	4.4 – 5.3	0.71
FL	10/10/2007 - 10/25/2021	0.40	4.0	3.0 – 4.4	1.50
MS	01/01/2010 - 01/05/2022	0.31	4.8	3.8 - 5.2	0.94
VA	01/01/2010 - 12/31/2021	0.32	4.4	3.5 – 4.8	0.75
NJ	07/27/2016 - 11/24/2021	0.34	3.8	2.8 – 4.1	0.70

EPE scenario used the measured precipitation record, while the non-EPE scenario was created by setting the precipitation to 0 for the heaviest rain day (September 12, 2013). Other parameters and input data are identical in both scenarios (Fig. 4). The modeled water-table displacement from the EPE scenario and the measured water-table displacement generally agree, with the modeled water table peak at \sim 25.0 m and the measured peak at \sim 25.2 m. The model, however, simulates the peak occurrence about 25 days after the EPE, whereas the field observations measured peak occurrence 14 days post-EPE. The two quantitative differences are likely due to the model assumptions of using a simple 1D model with two layers of similar hydraulic parameters. Nevertheless, the 1D model is a good assumption for the Betasso monitoring well as the well is located at a local drainage divide. The 1D results accomplish general agreement with field observations. Both the measured and the EPE modeled water table remained elevated for at least 1.6 years after the EPE, receding back to match the non-EPE model scenario water table in the spring of 2015 (Fig. 4).

3.2. Water-table displacement

3.2.1. Water-table displacement in response to EPE amount

Fig. 5 shows that for the 17 cases, modeled water tables were displaced by at least 0.65 m (WA) and at most by 2.40 m (CO). The average

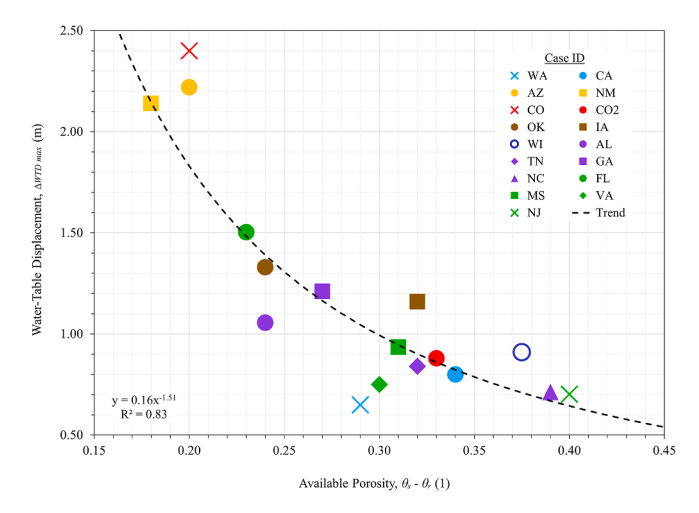


Fig. 6. Modeled maximum water-table displacement, $\Delta_{WTD~max}$ for each case as a function of the available porosity. (For interpretation of the references to colour in this figure legend, the reader is referred to the web version of this article.)

 Δ_{WTD} was 1.20 m. The case with the smallest EPE of 0.16 m (NM) produced a Δ_{WTD} of 2.14 m. The case with the largest EPE of 0.40 m (FL) produced a Δ_{WTD} of 1.50 m (Table 2). Three cases (AZ, NM, CO) show greater water-table displacements ($\Delta_{WTD} > 1.80$ m) for a given 1-day EPE amount, with an EPE of 0.16 m/d for the NM case, 0.18 m for the AZ case and 0.22 m for the CO case (Fig. 5). To better understand why Δ_{WTD} may be higher for the AZ, NM, CO cases, the unsaturated zone properties are considered in the following section.

3.2.2. Available porosity a control of water-table displacement

In the subsurface, water content, θ , is defined as $\theta = V_w / V_b$ where V_t is the total volume of the medium (i.e., soil or rock) and V_w is the volume of water (Freeze and Cherry, 1979). When all the pores in the medium are filled with water, the local water content equals porosity, $\theta = n$. In the unsaturated zone, θ is less than porosity, $\theta < n$ (Freeze and Cherry, 1979). For the cases considered, θ_r ranges from 0.03 (CO) to 0.26 (AL) and θ_s ranges from 0.25 (AZ) to 0.50 (AL). The difference, $(\theta_s - \theta_r)$, can be considered the available porosity of the unsaturated medium. Available porosity plays a role in the van Genuchten equations (equation (2)), where the available porosity controls the soil–water retention curve. These open voids are the fraction of the soil volume that is available to accept water (Nimmo, 2013).

Fig. 6 shows modeled Δ_{WTD} in response to EPE as a function of available porosity. Higher Δ_{WTD} occurs in cases with lower available

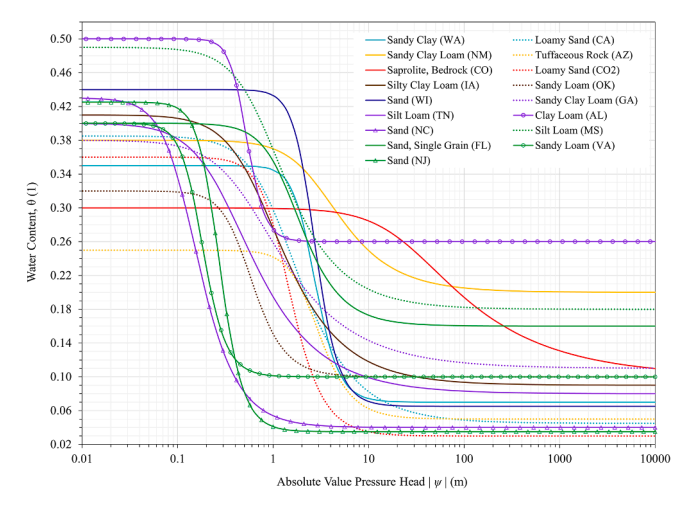


Fig. 7. Soil Water Retention Curves (SWRCs) from inverse modeling for the 17 study cases. (For interpretation of the references to colour in this figure legend, the reader is referred to the web version of this article.)

porosity. The three cases with the highest Δ_{WTD} (>1.8 m) had the smallest available porosity values, ranging from 0.18 (NM) to 0.20 (AZ, CO). The remaining 14 cases have available porosities between 0.23 and 0.40 and Δ_{WTD} values from 0.65 m (WA) to 1.50 m (FL). Of particular note are the CO and CO2 cases, with available porosities of 0.20 (CO) and 0.33 (CO2), and Δ_{WTD} of 2.40 (CO) and 0.88 (CO2) respectively. The CO case exhibits comparatively less available porosity and a high Δ_{WTD} (as verified by field measurements) while the CO2 case exhibits more available porosity and a smaller simulated Δ_{WTD} . Our model results suggest that in the unsaturated zone, available porosity exerts a strong control on water-table response to EPEs. The plotted trendline shows that a power function can explain 83 % of the variability, where less available porosity leads to higher water-table displacement and vice versa. Physically, the available porosity controls the amount of water required per unit volume of soil material to transition from partiallysaturated to fully-saturated. For a soil with a small available porosity, a small amount of water can quickly fill partially-saturated pores leading to large rise in Δ_{WTD} . For a soil with a large available porosity, the same amount of water results in a smaller rise in Δ_{WTD} . Thus, less available porosity (AZ, NM, CO) is correlated with larger Δ_{WTD} , and greater available porosity is correlated with smaller Δ_{WTD} .

3.2.3. Soil-water retention curves (SWRC) and water-table displacement

To further understand how Δ_{WTD} is affected by soil properties we consider the soil-water retention curve (SWRC) for each case. The SWRC relates the energy state of the pressure head, ψ to the local volumetric water content, θ , at equilibrium above the water table in a soil (van Genuchten, 1980). From the SWRCs of the soils (Fig. 7), it can be understood how the available porosity is a controlling factor of Δ_{WTD} , but also how the absolute porosity, (n), plays a role in influencing watertable displacement. The porosity ($\theta_s \sim n$) of the cases range from 0.25 (AZ) to 0.50 (AL). A lower n (Fig. 7) indicates that a smaller volume of pore space available to accommodate infiltrating water. The respective lower n of 0.25 (AZ) and 0.30 (CO) allows for larger Δ_{WTD} (Fig. 6). However, the next lowest n = 0.32 of the OK soil, does not exhibit the third largest Δ_{WTD} , instead the NM soil (greater n=0.38) does. This can be understood by examining the SWRCs (Fig. 7). The OK soil has a low n= 0.32, and a higher available porosity than the NM soil. Therefore, the OK soil has more pore space available for water to fill, inhibiting a larger Δ_{WTD} . Thus, the porosity and available porosity, can serve as a first-order indicator of how large Δ_{WTD} may be.

Once the water table has reached its peak displacement (Fig. 1c), the wetting process transitions into a drying process. The water table begins to recede, and the once saturated soil begins to lose water. For the purpose of this study, an increase in negative pressure head will be discussed as an increase in absolute value pressure head. This allows ψ to be plotted on a logarithmic scale (Fig. 7). An increase in absolute value pressure head results in a decrease in water content from θ_s . The α (m⁻¹) is inversely related to the air-entry pressure, denoting the physical setting at which there is enough pressure to empty the largest pore of the soil (Kosugi et al., 2002; Nimmo, 2013). Water in the pore space is subsequently replaced by air. As the soil dries and the $|\psi|$ becomes larger than the air-entry pressure, the water content decreases, depicted in a SWRC as a sloped line that could be gentle or steep depending on the $\theta - \psi$ relation. As the soil continues to dry and the pressure head becomes even larger, the water content decreases asymptotically towards the residual water content. The SWRC generally follows a smooth Zshaped curve (Fig. 7) between the bounds at θ_s and at θ_r , and the available porosity can be seen as the difference between these limits.

The soil–water retention curves of the 17 cases are spread across a wide range of available porosities (Fig. 7). Most of the soils exhibit a moderate to steep $\theta - \psi$ slope. The SWRC for the AZ, NM, and CO materials exhibit comparatively gentler slopes. Gentler SWRC slopes are indicative of saturation retention over greater changes in absolute value pressure head (Fig. 7). Most cases maintain full saturation up to a pressure head of $|\psi| \sim 0.1$ m. Two of the cases with larger Δ_{WTD} , AZ and

NM, maintain saturation until $|\psi|\sim 1.0$ m. In particular, the CO material remains saturated at $|\psi|>10$ m.

The SWRC also helps illustrate the relatively lower porosity $(n \sim \theta_s)$ of the materials with higher water-table displacements. For example, the porosity of the CO material is low $(n \sim 0.30)$ and the available porosity is even lower (0.20). The combination of low n and low available porosity suggests that a smaller volume of water is needed to raise the water table. Thus, the information provided by the SWRC for a soil, specifically the θ_s , θ_r , and $\theta-\psi$ relations can prove useful as first-order indicator when examining the potential water-table displacement of a soil responding to an EPE.

3.3. Water-table recession time controlled by saturated hydraulic diffusivity

3.3.1. Saturated hydraulic diffusivity

Water-table recession is governed by drainage over time in the saturated zone (Freeze and Cherry, 1979). After peak water-table displacement occurs, the water table recedes. We defined water-table recession time, t_{rec} , as the time it took for 95 % of the EPE-caused $\Delta_{WTD~max}$ to recede to non-EPE scenario levels. Depending on the Δ_{WTD} max of the soil, the 5 % displacement thresholds varied between 0.04 m and 0.13 m. In the saturated zone, the time it takes for water to flow a certain distance can be examined by considering the hydraulic diffusivity, D. The hydraulic diffusivity is a measure of the ability of a material to transfer water relative to its ability to store water. The $D(L^2/T)$ is a function of the fluid and medium properties of a saturated aquifer and can be calculated given the saturated hydraulic conductivity, K_s (L/ T), specific yield, S_y (dimensionless) and aquifer thickness, A_t (L). For this study, A_t was the distance from the water table to the bottom of the soil column. Thus, the estimated saturated aquifer thickness was, $A_t \sim$ 41–46 m for 16 cases and $A_t \sim 23$ m for the Betasso case. The specific yield, S_{ν} , is a storage term for unconfined aquifers, defined as the volume of water released from storage per unit surface area of aquifer per unit decline in the water table (Freeze and Cherry, 1979). S_v is approximately equal to the porosity, n, which can be equated to the saturated water content, θ_s . Therefore, D for the saturated aquifer was defined as:

$$D = \frac{K_s}{\theta_s/A_t} \tag{7}$$

The hydraulic diffusivity, D (m²/d) describes how fast a pressure pulse propagates through a saturated medium (Wang, 2020). We examined the water-table recession time (t_{rec}) as a function of D and

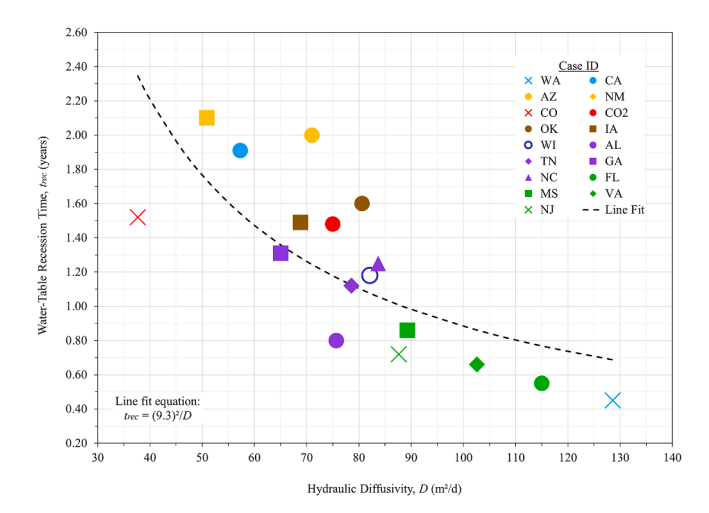


Fig. 8. Modeled recession time, t_{rec} versus the saturated hydraulic diffusivity, D (m²/d) for each case. (For interpretation of the references to colour in this figure legend, the reader is referred to the web version of this article.)

Soil Textural Triangle

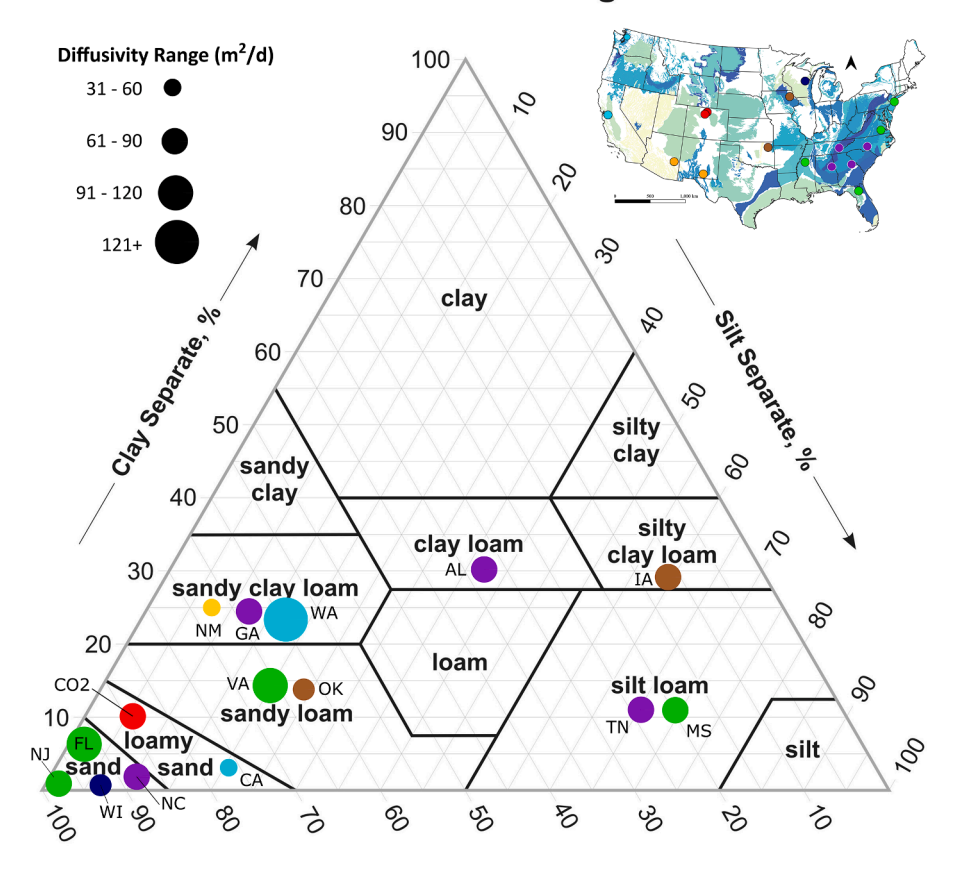


Fig. 9. Dots show soil texture class for soils used in this study, but do not specify clay-silt-sand percentages, which were not reported in site data. Circle size denotes range of diffusivity values for the soils considered. Not shown: AZ (tuffaceous rock) and CO (unweathered bedrock). Inset: Fig. 2 for reference. (For interpretation of the references to colour in this figure legend, the reader is referred to the web version of this article.)

Table 3 Average saturated hydraulic conductivity, K_s , porosity, n, diffusivity, D, and recession time, t_{rec} for each model case.

Case ID	Averaged Saturated Hydraulic Conductivity, K_s (m/d)	Porosity n	Diffusivity D (m ² /d)	Recession Time t _{rec} (yrs)
WA	1.00	0.35	128.57	0.45
CA	0.50	0.39	57.27	1.91
AZ	0.40	0.25	71.00	2.00
NM	0.45	0.38	50.92	2.10
CO	0.50	0.30	37.67	1.52
CO2	0.60	0.36	75.00	1.48
OK	0.60	0.34	80.60	1.60
IA	0.65	0.41	68.80	1.49
WI	0.80	0.44	82.10	1.18
AL	0.85	0.50	76.65	0.80
TN	0.70	0.40	78.58	1.12
GA	0.60	0.38	65.05	1.31
NC	0.80	0.43	83.68	1.25
FL	1.00	0.39	115.00	0.55
MS	0.95	0.49	89.25	0.86
VA	0.90	0.40	102.60	0.66
NJ	0.85	0.44	87.63	0.72

found that t_{rec} varied from 0.40 years to 2.10 years for D values ranging from 37 m²/d to 129 m²/d (Fig. 8). For cases with smaller D values (<80 m²/d), the water table took longer to recede to non-EPE scenario levels (Fig. 8), with t_{rec} ranging between 1.49 years (IA) to 2.10 years (NM). Where D was larger (>80 m²/d), recession times were shorter, ranging from 0.45 years (WA) to 1.25 years (NC). Given that D represents a

characteristic length squared over a characteristic time (Bruce and Klute, 1956), the following equation was fit to the data:

$$t_{rec} = \frac{L^2}{D} \tag{8}$$

where t_{rec} is recession time (years), L is a fitting parameter representing a characteristic length (m), and D is the saturated hydraulic diffusivity (m 2 /d). The best-fitting parameter for the data was L=9.30 m, representing the characteristic distance that the EPE signal may have diffused through in the subsurface. The fitted line highlights a negative trend: longer recession times are correlated with smaller D values, while shorter recession times are correlated with larger D values.

Fig. 8 shows that the slope of dt_{rec}/dD steepens as D become smaller, which could be important for cases with smaller K_s values than those considered here. In contrast, the slope is gentler for larger D values, which suggests that the recession time may reach a limiting value as D increases. Based on the results, we hypothesize that a recession time minimum may exist, which we define as the minimum amount of time it may take for the water table affected by an EPE to recede back to pre-EPE levels. This minimum may be \sim 0.4 years. More research is needed to explore this idea.

The plot of D versus t_{rec} (Fig. 8) shows a strong correlation for larger diffusivities, but the correlation is scattered for smaller diffusivities. Recession times lasting longer than 1.3 years with diffusivity values less than ~80 m²/d are not well explained by the line fit equation. Recession times longer than ~1.45 years are attributed to smaller diffusivities in the range of 37 ~ 80 m²/d and lower values of porosity (θ_s ~ 0.33) on average (Table 3, Fig. 8). Recession times shorter than ~1.30 years are

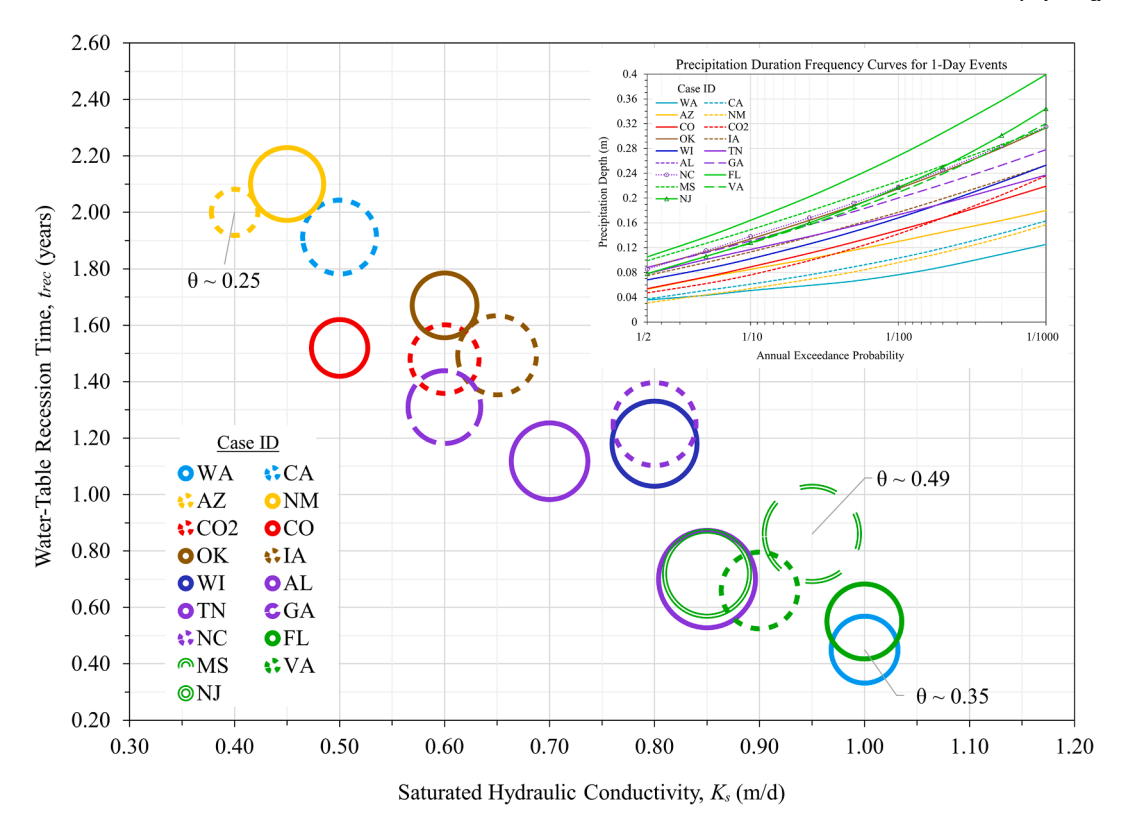


Fig. 10. Modeled values of recession time, t_{rec} versus saturated hydraulic conductivity, K_s (m/d) values of each case. Symbol sized according to θ_s of each case. Inset: Fig. 2 for reference. (For interpretation of the references to colour in this figure legend, the reader is referred to the web version of this article.)

attributed to larger diffusivities (65–130 m²/d) and higher porosity ($\theta_s \sim 0.42$) on average (Table 3, Fig. 8).

To further explore the relation between D and soil/rock properties, we plotted the respective soil types onto a modified version of the U.S. Department of Agriculture's (U.S. Department of Agriculture, 1987) soil textural triangle classification system (Fig. 9).

The hydraulic diffusivities of the 17 cases cover a wide range of soil textures (Fig. 9). Sandier soils tend to be moderately to well-drained, which is reflected by larger *D* values (Fig. 9). Soils with mixed amounts of clay, silt, and sand, drain at variable rates, which is reflected by the range of recession times for similar *D* values (Fig. 9). We acknowledge that more data could be helpful in understanding the connections between soil materials and diffusivity, and urge future studies to consider clay-rich soils, which are not well-represented in this study.

3.3.2. Saturated hydraulic conductivity

The difference between high and low diffusivities is implicitly related to the soil hydraulic properties (K_s, θ_s) that construct the D (equation (7)). The K_s and t_{rec} are inversely correlated (Fig. 10), with circle size defined by the value of θ_s . Cases with smaller K_s and θ_s values (i.e. tuffaceous rock, unweathered bedrock, sandy clay loam) have smaller diffusivities. Physically, this suggests that when infiltration from an EPE reaches the saturated zone, the pressure pulse takes more time to propagate through the medium, thus resulting in longer recession times. In contrast, cases with larger K_s and θ_s values (i.e., sandy soils) allow for water to be transmitted relatively faster through the medium, indicating a larger diffusivities and shorter recession times.

From a climate perspective, cases with smaller K_s and longer recession times are also those with lower 1-day EPE amounts, which may reflect drier soils (low- to mid- K_s) and drier climates (Fig. 10). Cases with larger K_s and shorter recession times are also those with higher 1-day EPE amounts, which may reflect more conductive soils and wetter climates (Fig. 10).

Provided that recession times for water tables remain elevated for 0.4 years to 2.1 years after an EPE, the elevated water tables could be a welcome opportunity for communities-in-need to extract water resources. In terms of direct extraction, communities in mountainous regions and near ephemeral streams are most likely to benefit. Done efficiently, this recession time window could be exploited during summer months when little to no rain is expected in generally drier regions (i.e., southwest U.S, drier parts of Australia, Africa). For example, if soils with lower diffusivities, in dry regions, experience EPEs, then water could be pumped out for storage to be used at a later time. Indirectly, elevated water tables could also provide more baseflow to streams, rivers, and lakes, which would subsequently benefit more communities.

With climate change affecting the annual snow-to-rainfall precipitation ratios (Trenberth, 2011), elevated water tables could also be tapped by wetter regions when less precipitation is available (Wilkinson and Cooper, 1993). This could prove of great benefit for areas expected to suffer from elevation-dependent warming (Pepin et al., 2015). Overall, the ability to pump water resources after EPEs could help modulate water resource extraction based on community need.

3.4. Future considerations and implications

A future in which EPEs become more frequent could lead to an increased likelihood of larger flooding events (Wasko et al., 2021; Geris et al., 2022) and water quality issues (Nguyen et al., 2021; Geris et al., 2022). For example, Geris et al. (2022) found that an EPE in a semi-arid region was simultaneously responsible for 1) widespread flooding, 2) high groundwater recharge, and 3) subsurface contaminant mobilization due to elevated water tables promoting local landfill drainage. Subsurface response to EPEs has also resulted in increased likelihood of slope failures (Smith et al., 2017; Hou et al., 2021), and building foundation issues (Garcia-Gaines and Frankenstein, 2015).

In recognition of the predicted increase and frequency of EPEs (Du

et al., 2022), it is important to identify the controls that cause watertable displacement variations from one soil type to another. Our approach highlights the importance of organized soil sample datasets like UNSODA (Nemes et al., 2001). In the absence of more intensive field studies, $\theta(\psi)$ and K_s from soil sample catalogs may serve as empirical controls on water-table response to EPEs in future modeling efforts. In addition to the data discussed in this study, UNSODA contains soil data for >100 sites in over 20 countries across the European, African, Asian and Australian continents (Nemes et al., 2001). Regions at risk of EPEs (Sun et al., 2021) could undergo this analysis and examine whether: (1) the available porosity of a soil controls water-table displacement and (2) how the K_s and D controls water-table recession time. Such tests could indicate if the relations highlighted here could be more generally applicable globally.

4. Conclusion

As the link between climate and groundwater, soil hydraulic properties that control subsurface response warrant greater attention in the face of increasingly likely EPEs. In the unsaturated zone, our results show that across varying soil-types and precipitation cases, EPEs cause significant variations in water-table displacement and recession times. Future studies can be broadened to explore water-table response and recession time in soil properties and precipitation space.

4.1. Summary

We examined water-table response, namely water-table displacement, and recession time to EPE-induced infiltration. We used water content and pressure head data from 17 cases along with inverse modeling to determine soil—water retention curves. We used a 1d modeling approach to show that water-table response to EPEs can be significant and to explore how varied materials (hydraulic properties) affect the response. For each case, the transient modeling included the "non-EPE" scenario where no EPE was applied and the "EPE" scenario where the 1-day EPE was added to the non-EPE scenario. The modeling results of the non-EPE and EPE scenarios were compared to determine the Δ_{WTD} and t_{rec} . The following conclusions are drawn from the results of this study:

- Subsurface response to EPEs led to water-table displacements ranging from 0.6 to 2.4 m across the 17 study cases.
- Available porosity in the unsaturated zone exerts a strong control on water-table displacement. Low available porosity leads to larger water-table displacement and vice versa.
- Saturated hydraulic diffusivity is a major control of water-table recession time, t_{rec} . A factor of three variation in D caused about a factor of four variation in recession times.
- Results hint at a limiting value for the recession time, set by the hydraulic diffusivity, *D*.

We further urge field collection, lab analysis, and consideration of soil hydraulic property data to validate future modeling studies related to water table fluctuations and groundwater recharge.

 ${\it CRediT\ authorship\ contribution\ statement}$

Claudia R. Corona: Conceptualization, Investigation, Methodology, Software, Data curation, Validation, Writing – original draft, Writing – review & editing. Shemin Ge: Conceptualization, Investigation, Supervision, Writing – review & editing. Suzanne P. Anderson: Conceptualization, Investigation, Supervision, Writing – review & editing.

Declaration of Competing Interest

The authors declare that they have no known competing financial

interests or personal relationships that could have appeared to influence the work reported in this paper.

Data availability

Data will be made available on request.

Acknowledgements

This research was supported by the National Science Foundation, Division of Earth Sciences, Hydrologic Sciences program under Grant EAR-1834290.

References

- Alley, W.M., 2002. Flow and storage in groundwater systems. Science 296, 1985–1990. https://doi.org/10.1126/science.1067123.
- Anderson, S.P., Ragar, D., 2022. Betasso Well Water Levels (BT_GW_1_Pducer) (2013-2018), Hydroshare, http://www.hydroshare.org/resource/ 6f8ee0a3ce5c45e4870976bb3d8d1bfc. Accessed: 07/25/2022.
- Anderson, S.P., Anderson, R.S., Tucker, G.E., Dethier, D.P., 2013. Critical zone evolution: Climate and exhumation in the Colorado Front Range, in: Classic Concepts and New Directions: Exploring 125 Years of GSA Discoveries in the Rocky Mountain Region. Geological Society of America. https://doi.org/10.1130/2013.0033(01).
- Anderson, S.P., Rock, N., Ragar, D., 2022. BCCZO Meteorology, Air Temperature (BT_Met) Betasso (2009-2020). URL https://www.hydroshare.org/resource/6bf3e44b9de344749d8f665e139e7311/ (accessed 7.31.22).
- Boas, T., Mallants, D., 2022. Episodic extreme rainfall events drive groundwater recharge in arid zone environments of central Australia. J. Hydrol.: Reg. Stud. 40, 101005 https://doi.org/10.1016/j.ejrh.2022.101005.
- Bruce, R.R., Klute, A., 1956. The measurement of soil moisture diffusivity. Soil Sci. Soc. Am. J. 20, 458–462. https://doi.org/10.2136/sssaj1956.03615995002000040004x.
- Cary, J.W., Hayden, C.W., 1973. An index for soil pore size distribution. Geoderma 9, 249–256. https://doi.org/10.1016/0016-7061(73)90026-8.
- Corona, C.R., Ge, S., 2022. Examining subsurface response to an extreme precipitation event using HYDRUS-1D. Vadose Zone J. 15 https://doi.org/10.1002/vzj2.20189.
- Corona, C.R., Gurdak, J.J., Dickinson, J.E., Ferré, T.P.A., Maurer, E.P., 2018. Climate variability and vadose zone controls on damping of transient recharge. J. Hydrol. 561, 1094–1104. https://doi.org/10.1016/j.jhydrol.2017.08.028.
- Crosbie, R.S., 2003. Regional Scaling of Groundwater Recharge (Doctoral Dissertation). University of Newcastle, Newcastle, Australia.
- Dieter, C.A., Maupin, M.A., Caldwell, R.R., Harris, M.A., Ivahnenko, T.I., Lovelace, J.K., Barber, N.L., Linsey, K.S., 2018. Estimated use of water in the United States in 2015 (U.S. Geological Survey Circular No. 1141), Water Availability and Use Science Program. U.S. Geological Survey, Reston, Virginia. https://doi.org/10.3133/cir1441.
- Du, H., Donat, M.G., Zong, S., Alexander, L.V., Manzanas, R., Kruger, A., Choi, G., Salinger, J., He, H.S., Li, M.-H., 2022. Extreme precipitation on consecutive days occurs more often in a warming climate. Bull. Am. Meteorol. Soc. 103, E1130–E1145. https://doi.org/10.1175/BAMS-D-21-0140.1.
- Fiore, A.R., Ashland, F.X., Reilly, P.A., Mirus, B.B., 2021. Hydrologic, slope movement, and soil property data from the coastal bluffs of the Atlantic Highlands, New Jersey, 2016-2018. U.S. Geological Survey Data Release. https://doi.org/10.5066/PPA601HC.
- Freeze, R.A., 1969. The mechanism of natural ground-water recharge and discharge: 1. One-dimensional, vertical, unsteady, unsaturated flow above a recharging or discharging ground-water flow system. Water Resour. Res. 5, 153–171. https://doi.org/10.1029/WR005i001p00153.
- Freeze, R.A., Cherry, J.A., 1979. Groundwater, 1st ed. Prentice-Hall, Inc., Englewood Cliffs, New Jersey, 07632, University of British Columbia, University of Waterloo.
- Garcia-Gaines, R., Frankenstein, S., 2015. USCS and the USDA Soil Classification System: Development of a Mapping Scheme. (No. ERDC/CRREL TR-15-4). U.S. Army Engineer Research and Development Center, Vicksburg, MS. https://erdc-library. erdc.dren.mil/jspui/bitstream/11681/5485/1/ERDC-CRREL-TR-15-4.pdf.
- Geris, J., Comte, J.-C., Franchi, F., Petros, A.K., Tirivarombo, S., Selepeng, A.T., Villholth, K.G., 2022. Surface water-groundwater interactions and local land use control water quality impacts of extreme rainfall and flooding in a vulnerable semiarid region of Sub-Saharan Africa. J. Hydrol. 609, 127834 https://doi.org/10.1016/ j.jhydrol.2022.127834.
- Gochis, D., Schumacher, R., Friedrich, K., Doesken, N., Kelsch, M., Sun, J., Ikeda, K., Lindsey, D., Wood, A., Dolan, B., 2015. The great Colorado flood of September 2013. Bull. Am. Meteorol. Soc. 96, 1461–1487. https://doi.org/10.1175/BAMS-D-13-00241
- Golian, M., Katibeh, H., Najafi, Z., Saadat, H., Saffarzadeh, A., Ahmadi, A., Khazaei, M., Sametzadeh, E., 2021. Large-scale replenishment of groundwater depletion by long-lived extreme rainstorms in arid regions: case study of the 2019 floods in Iran. Hydrgeol. J. https://doi.org/10.1007/s10040-021-02370-8.
- Green, T.R., Taniguchi, M., Kooi, H., Gurdak, J.J., Allen, D.M., Hiscock, K.M., Treidel, H., Aureli, A., 2011. Beneath the surface of global change: impacts of climate change on groundwater. J. Hydrol. 405, 532–560. https://doi.org/10.1016/j. jhydrol.2011.05.002.

- Healy, R.W., Cook, P.G., 2002. Using groundwater levels to estimate recharge. Hydrgeol. J. 10, 91–109. https://doi.org/10.1007/s10040-001-0178-0.
- Hopmans, J.W., Stricker, J.N.M., 1989. Stochastic analysis of soil water regime in a watershed. J. Hydrol. 105, 57–84. https://doi.org/10.1016/0022-1694(89)90096-6.
- Hosking, J.R.M., Wallis, J.R., 1997. Regional Frequency Analysis: An Approach Based on L-Moments. Cambridge University Press, New York, New York.
- Hosking, J.R.M., Wallis, J.R., Wood, E.F., 1985. Estimation of the generalized extremevalue distribution by the method of probability-weighted moments. Technometrics 27, 251–261. https://doi.org/10.1080/00401706.1985.10488049.
- Hou, X., Li, T., Qi, S., Guo, S., Li, P., Xi, Y., Xing, X., 2021. Investigation of the cumulative influence of infiltration on the slope stability with a thick unsaturated zone. Bull. Eng. Geol. Environ. 80, 5467–5480. https://doi.org/10.1007/s10064-021-02287-2.
- Jasechko, S., Taylor, R.G., 2015. Intensive rainfall recharges tropical groundwaters. Environ. Res. Lett. 10, 124015 https://doi.org/10.1088/1748-9326/10/12/124015.
- Joachim, D.R., Gotkowitz, M.B., Potter, K.W., Bradbury, K.R., Vavrus, S.J., Loheide, S.P., 2011. Forecasting impacts of extreme precipitation events on Wisconsin's groundwater levels. Wisconsin Geological and Natural History Survey 22. https://wri.wisc.edu/wp-content/uploads/FinalWR09R005.pdf.
- Kosugi, K., Hopmans, J.W., Dane, J.H., 2002. 3.3.4 Parametric Models. Methods of Soil Analysis: Part 4 Physical Methods 5, 739–757.
- Langston, A.L., Tucker, G.E., Anderson, R.S., Anderson, S.P., 2015. Evidence for climatic and hillslope-aspect controls on vadose zone hydrology and implications for saprolite weathering: Climatic Control on Vadose Zone Moisture. Earth Surf. Process. Landforms 40, 1254–1269. https://doi.org/10.1002/esp.3718.
- Lehmann, J., Coumou, D., Frieler, K., 2015. Increased record-breaking precipitation events under global warming. Clim. Change 132, 501–515. https://doi.org/ 10.1007/s10584-015-1434-y.
- Leterme, B., Mallants, D., Jacques, D., 2012. Sensitivity of groundwater recharge using climatic analogues and HYDRUS-1D. Hydrol. Earth Syst. Sci. 16, 2485–2497. https://doi.org/10.5194/hess-16-2485-2012.
- Li, C., Zwiers, F., Zhang, X., Chen, G., Lu, J., Li, G., Norris, J., Tan, Y., Sun, Y., Liu, M., 2019. Larger increases in more extreme local precipitation events as climate warms. Gephys. Res. Lett. 46, 6885–6891. https://doi.org/10.1029/2019GL082908.
- Maupin, M.A., 2018. Summary of estimated water use in the United States in 2015 (No. 2018–3035), Fact Sheet. US Geological Survey, Reston, VA. https://doi.org/10.3133/fs20183035.
- Miguez-Macho, G., Fan, Y., Weaver, C.P., Walko, R., Robock, A., 2007. Incorporating water table dynamics in climate modeling: 2. Formulation, validation, and soil moisture simulation. J. Geophys. Res. Atmos. 112. https://doi.org/10.1029/ 2006JD008112.
- Mualem, Y., 1976. A new model for predicting the hydraulic conductivity of unsaturated porous media. Water Resour. Res. 12, 513–522. https://doi.org/10.1029/ WR012i003p00513.
- Myhre, G., Alterskjær, K., Stjern, C.W., Hodnebrog, Ø., Marelle, L., Samset, B.H., Sillmann, J., Schaller, N., Fischer, E., Schulz, M., Stohl, A., 2019. Frequency of extreme precipitation increases extensively with event rareness under global warming. Sci. Rep. 9, 16063. https://doi.org/10.1038/s41598-019-52277-4.
- Nemes, A., Schaap, M.G., Leij, F.J., Wösten, J.H.M., 2001. Description of the unsaturated soil hydraulic database UNSODA version 2.0. J. Hydrol. 251, 151–162. https://doi. org/10.1016/S0022-1694(01)00465-6.
- Neto, D.C., Chang, H.K., van Genuchten, M.T., 2016. A mathematical view of water table fluctuations in a shallow aquifer in brazil: ground water. Groundwater 54, 82–91. https://doi.org/10.1111/gwat.12329.
- Nguyen, H.H., Peche, A., Venohr, M., 2021. Modelling of sewer exfiltration to groundwater in urban wastewater systems: a critical review. J. Hydrol. 596, 126130 https://doi.org/10.1016/j.jhydrol.2021.126130.
- Nimmo, J.R., 2013. Porosity and Pore Size Distribution: Reference Module in Earth Systems and Environmental Sciences. Elsevier 3, 1–10. http://dx.doi.org/10.1016/ B978-0-12-409548-9.05265-9.
- NOAA, 2017. National Oceanic and Atmospheric Association (NOAA) Atlas 14 Point Precipitation Frequency Estimates, https://hdsc.nws.noaa.gov/hdsc/pfds/pfds_map_cont.html. Accessed: 04/06/2022.
- NRCS, 2022a. Official Soil Series Description by List. URL https://soilseries.sc.egov.usda. gov/ (accessed 7.31.22).
- NRCS, 2022b. Official Soil Series Description by List: Webster Series. URL https://soilseries.sc.egov.usda.gov/OSD_Docs/w/webster.html (accessed 7.31.22).
- NRCS, 2022c. Official Soil Series Description by List: Glendale Series. URL https://soilseries.sc.egov.usda.gov/OSD_Docs/g/glendale.html (accessed 7.31.22).
- NRCS, 2022d. Official Soil Series Description by List: Konawa Series. URL https://soilseries.sc.egov.usda.gov/OSD_Docs/K/KONAWA.html (accessed 7.31.22).
- NRCS, 2022e. Official Soil Series Description by List: Fullerton Series. URL https://soilseries.sc.egov.usda.gov/OSD_Docs/f/fullerton.html (accessed 7.31.22).Suns.
- NRCS, 2022f. Official Soil Series Description by List: Plainfield Series. URL https://soilseries.sc.egov.usda.gov/OSD_Docs/p/plainfield.html (accessed 7.31.22).
- Pendergrass, A.G., Knutti, R., 2018. The uneven nature of daily precipitation and its change. Geophys. Res. Lett. 45, 11980–11988. https://doi.org/10.1029/ 2018GL080298.
- Pepin, N., Bradley, R.S., Diaz, H.F., Baraër, M., Caceres, E.B., Forsythe, N., Fowler, H., Greenwood, G., Hashmi, M.Z., Liu, X.D., Miller, J.R., 2015. Elevation-dependent warming in mountain regions of the world. Nat. Clim. Change, Mountain Research Initiative EDW Working Group 5, 424–430. https://doi.org/10.1038/nclimate2563.
- Perica, S., Martin, D., Pavlovic, S., Roy, I., St. Laurent, M., Trypaluk, C., Unruh, D., Yekta, M., Bonnin, G., 2013. NOAA Atlas 14 Precipitation-Frequency Atlas of the United States Volume 9 Version 2.0: Southeastern States (Alabama, Arkansas, Florida,

- Georgia, Louisiana, Mississippi) (Volume No. 9). National Weather Service. https://www.weather.gov/media/owp/oh/hdsc/docs/Atlas14_Volume9.pdf.
- Prein, A.F., Rasmussen, R.M., Ikeda, K., Liu, C., Clark, M.P., Holland, G.J., 2017. The future intensification of hourly precipitation extremes. Nat. Clim. Chang. 7, 48–52. https://doi.org/10.1038/nclimate3168.
- Reitz, M., Sanford, W.E., Senay, G.B., Sanford, W.E., 2017. Combining remote sensing and water-balance evapotranspiration estimates for the conterminous United States. Remote Sens. (Basel) 9, 1181. https://doi.org/10.3390/rs9121181.
- Richards, L., 1931. Capillary conduction of liquids in porous mediums. Physics 1, 318-333.
- Sanford, W.E., Selnick, D.L., 2013. Estimation of evapotranspiration across the conterminous United States using a regression with climate and land-cover data. J. Am. Water Resour. Assoc. 49, 217–230. https://doi.org/10.1111/jawr.12010.
- Scanlon, B.R., Zhang, Z., Save, H., Sun, A.Y., Schmied, H.M., van Beek, L.P., Wiese, D.N., Wada, Y., Long, D., Reedy, R.C., 2018. Global models underestimate large decadal declining and rising water storage trends relative to GRACE satellite data. Proc. Natl. Acad. Sci. 115, E1080–E1089.
- Šimůnek, J., Van Genuchten, M.T., Sejna, M., 2005. The HYDRUS-1D software package for simulating the one-dimensional movement of water, heat, and multiple solutes in variably-saturated media. University of California-Riverside Research Reports 3, 1–240. https://www.pc-progress.com/Downloads/Pgm_hydrus1D/HYDRUS1D-4.08.pdf.
- Smith, J.B., Baum, R.L., Mirus, B.B., Michel, A.R., Stark, B., 2017. Results of Hydrologic Monitoring on Landslide-prone Coastal Bluffs near Mukilteo, Washington (USGS Numbered Series No. 2017–1095), Open-file report. U.S. Geological Survey, Reston, VA. https://doi.org/10.3133/ofr20171095.
- Sun, Q., Zhang, X., Zwiers, F., Westra, S., Alexander, L.V., 2021. A global, continental, and regional analysis of changes in extreme precipitation. J. Clim. 34, 243–258. https://doi.org/10.1175/JCLI-D-19-0892.1.
- Tashie, A.M., Mirus, B.B., Pavelsky, T.M., 2016. Identifying long-term empirical relationships between storm characteristics and episodic groundwater recharge. Water Resour. Res. 52, 21–35. https://doi.org/10.1002/2015WR017876.
- Thomas, B., Behrangi, A., Famiglietti, J., 2016. Precipitation intensity effects on groundwater recharge in the southwestern United States. Water 8, 90. https://doi. org/10.3390/w8030090.
- Trenberth, K., 2011. Changes in precipitation with climate change. Climate Res. 47, 123–138. https://doi.org/10.3354/cr00953.
- U.S. Geological Survey, 2003. Principal Aquifers of the 48 Conterminous United States, Hawaii, Puerto Rico, and the U.S. Virgin Islands. Water Mission Area NSDI Node. https://water.usgs.gov/GIS/metadata/usgswrd/XML/aquifers_us.xml. Accessed: 04/20/2022
- van Genuchten, M.T., 1980. A closed-form equation for predicting the hydraulic conductivity of unsaturated soils. Soil Sci. Soc. Am. J. 44, 892. https://doi.org/ 10.2136/sssai1980.03615995004400050002x.
- Vereecken, H., Huisman, J.A., Hendricks Franssen, H.J., Brüggemann, N., Bogena, H.R., Kollet, S., Javaux, M., van der Kruk, J., Vanderborght, J., 2015. Soil hydrology: recent methodological advances, challenges, and perspectives. Water Resour. Res. 51, 2616–2633. https://doi.org/10.1002/2014WR016852.
- Wang, H., Gao, J.E., Zhang, M., Li, X., Zhang, S., Jia, L., 2015. Effects of rainfall intensity on groundwater recharge based on simulated rainfall experiments and a groundwater flow model. Catena 127, 80–91. https://doi.org/10.1016/j. catena.2014.12.014.
- Wang, H., 2020. Groundwater Storage in Confined Aquifers. The Groundwater Project, Guelph, Ontario, Canada. https://gw-project.org/books/groundwater-storage-inconfined-aquifers/.
- Wasko, C., Nathan, R., Stein, L., O'Shea, D., 2021. Evidence of shorter more extreme rainfalls and increased flood variability under climate change. J. Hydrol. 603, 12. https://doi.org/10.1016/j.jhydrol.2021.126994.
- Westenbroek, S.M., Kelson, V.A., Dripps, W.R., Hunt, R.J., Bradbury, K.R., 2010. SWB–A Modified Thornthwaite-Mather Soil-Water-Balance Code for Estimating Groundwater Recharge. US Department of the Interior, US Geological Survey, Ground Resources Program.
- Westra, S., Alexander, L.V., Zwiers, F.W., 2013. Global increasing trends in annual maximum daily precipitation. J. Clim. 26, 3904–3918. https://doi.org/10.1175/ ICLL D. 12.00502.1
- Wilkinson, W.B., Cooper, D.M., 1993. The response of idealized aquifer/river systems to climate change. Hydrol. Sci. J. 38, 379–390. https://doi.org/10.1080/ 026266693099492688
- Wittenberg, H., Aksoy, H., Miegel, K., 2019. Fast response of groundwater to heavy rainfall. J. Hydrol. 571, 837–842. https://doi.org/10.1016/j.jhydrol.2019.02.037.
- Wu, W., Geller, M.A., Dickinson, R.E., 2002. The response of soil moisture to long-term variability of precipitation. J. Hydrometeorol. 3, 604–613. https://doi.org/10.1175/ 1525-7541(2002)003<0604:TROSMT>2.0.CO;2.
- Youngs, E.G., 1988. Soil physics and hydrology. J. Hydrol. 100, 411–431. https://doi. org/10.1016/0022-1694(88)90194-1.
- Zhang, J., Felzer, B.S., Troy, T.J., 2016. Extreme precipitation drives groundwater recharge: the Northern High Plains Aquifer, central United States, 1950–2010: Extreme Prep Drives GWR: The NHP Aquifer, Central US, 1950–2010. Hydrol. Process. 30, 2533–2545. https://doi.org/10.1002/hyp.10809.
- Zheng, W., Wang, S., Sprenger, M., Liu, B., Cao, J., 2019. Response of soil water movement and groundwater recharge to extreme precipitation in a headwater catchment in the North China Plain. J. Hydrol. 576, 466–477. https://doi.org/ 10.1016/j.jhydrol.2019.06.071.